Novel LncRNA OXCT1-AS1 Indicates Poor Prognosis and Contributes to Tumorigenesis by Regulating miR-195/CDC25A Axis in Glioblastoma

Chen Zhong
Zhejiang University School of Medicine Second Affiliated Hospital
Qian Yu
Zhejiang University School of Medicine Second Affiliated Hospital
Shengjun Zhou
Zhejiang University School of Medicine Second Affiliated Hospital
Yucong Peng
Zhejiang University School of Medicine Second Affiliated Hospital
Zhendong Liu
First Affiliated Hospital of Harbin Medical University
Yong Deng
Zhejiang University School of Medicine Second Affiliated Hospital
Leiguang Guo
Zhejiang University School of Medicine Second Affiliated Hospital
Shiguang Zhao
First Affiliated Hospital of Harbin Medical University
Gao Chen (zcjy0529@163.com)
Zhejiang University School of Medicine Second Affiliated Hospital

Research

Keywords: Glioblastoma, Competing endogenous RNA network, Long noncoding RNA, OXCT1-AS1, Proliferation

Posted Date: December 28th, 2020

DOI: https://doi.org/10.21203/rs.3.rs-130876/v1

Version of Record: A version of this preprint was published at Journal of Experimental & Clinical Cancer Research on April 8th, 2021. See the published version at https://doi.org/10.1186/s13046-021-01928-4.

Abstract

Background

It's well known that long noncoding RNAs (lncRNAs) contribute to multiple biological processes of human glioblastoma (GBM). However, identifying a specific lncRNA target is still the major difficulty. In this study, bioinformatics methods and competing endogenous RNA network (ceRNA) regulatory rules was used to identify GBM related lncRNAs, and found OXCT1 antisense RNA 1 (OXCT1-AS1) may acted as a potential therapeutic target for treatment of glioma.

Methods

Based on the Gene Expression Omnibus (GEO) date set, we identified differential lncRNAs, microRNAs and mRNAs and constructed a lncRNA associated ceRNA network.

Novel lncRNA OXCT1-AS1 was proposed to exercise its function as a ceRNA, and its potential targeted miRNAs was predicted through the database LncBase Predicted v.2. The expression pattern of OXCT1-AS1 was measured in glioma and normal tissue samples. Effect of OXCT1-AS1 on glioma cells were checked by cell count kit 8 assay, cell clone formation assay, transwell assay and flow cytometry in vitro, respectively. The dual-luciferase activity assay was performed to investigate the potential mechanism of ceRNA network. Finally, orthotopic mouse models of glioma was created to evaluate the influence of OXCT1-AS1 on tumor growth in vivo.

Results

In this study, it was found that the expression of lncRNA OXCT1-AS1 is upregulated in both The Cancer Genome Atlas (TCGA) GBM cases and GBM tissue samples we collected, and a high expression of OXCT1-AS1 predicts poor prognosis of gliomas. Suppressing OXCT1-AS1 expression significantly decreased the proliferation of GBM cells and inhibited cell migration and invasion. We further investigated the potential mechanism and found OXCT1-AS1 may acted as a ceRNA of miR-195 to enhance CDC25A expression and attenuate glioma cells progression. Finally, knocking down of OXCT1-AS1 notably attenuated the severity of glioma in vivo.

Conclusion

OXCT1-AS1 inhibited glioma progression by regulating miR-195-5p/ CDC25A axis and can be a specific tumor marker and a novel potential therapeutic target for glioma treatment.

Introduction

Glioma is an aggressive subtype of primary brain tumor with an extremely poor prognosis, in which GBM is the most severe manifestation, accounts for approximately 1/5–1/4 of the primary intracranial malignancies [1, 2]. Patients with GBM suffer from a poor prognosis, and the 5-year survival rate is less than 10% [3, 4]. The prognosis of patients diagnosed with malignant gliomas remains grave although treatments such as radical surgery, radiotherapy, and chemotherapy are of value in the management of these tumors [5]. Moreover, prognostic biomarkers and therapeutic targets for gliomas have not been fully characterized [6, 7]. Therefore, it is necessary to identify novel biomarkers in glioma, as well as reveal the molecular mechanism that underlies glioma progression, which may be beneficial for the early diagnosis and effective treatment of the disease.

In eukaryotic cell genome, more than 90% human transcripts are found limited protein-coding capacity, but encoded non-coding RNA, including microRNA (miRNA), lncRNA, and circular RNA (circRNA) [8-10]. LncRNAs are non-coding RNA molecules of more than 200 nucleotides in length, transcribed by RNA polymerase II and exert several regulatory functions, at both transcriptional and post-transcriptional level [11]. Although lncRNAs do not have the ability of protein coding, they can regulate gene expression in various manners, such as genome modification, transcriptional activation, transcriptional interference and chromosome sedimentation [12, 13]. Growing numbers of evidences showed that the abnormal expression of lncRNAs is closely related to the pathogenesis, progression and prognosis of malignant tumors including GBM [14, 15]. Mechanistically, the ceRNA hypothesis suggests that lncRNAs can function as competing endogenous RNAs in human multiple malignancies to regulate miRNA-mRNA axis [16, 17]. To better understand the pathological process of GBM at genome level and identify new and specific lncRNA targets, we launched this research.

As for our present study, we constructed the lncRNA related ceRNA network in GBM and identified lncRNA OXCT1-AS1 might be the specific prognostic biomarker and therapeutic target in GBM. From TCGA and quantitative real-time PCR (qRT-PCR) assays, we found that the expression of OXCT1-AS1 was significantly decreased in GBM tissue samples and cell lines and the patients with the higher

OXCT1-AS1 expression have the worse prognosis. Additionally, we demonstrated that OXCT1-AS1 promote GBM proliferation through regulating miR-195/CDC25A axis in GBM. Our research firstly reported the expression pattern, biological function and potential regularly mechanism of lncRNA OXCT1-AS1 in GBM and may provide a novel diagnostic biomarker and therapeutic target for GBM.

Materials And Methods

Data collection

Series matrix files of GSE4290 dataset which contained mRNA microarray data of 23 epileptic tissues and 81 GBM [18], GSE90603 dataset which contained miRNA microarray data of 16 fresh-frozen GBM multiforme samples and 7 healthy brain tissues and GSE104267 dataset which contained mRNA microarray data of 9 tumors and 3 healthy tissues were downloaded from the GEO database (https://www.ncbi.nlm.nih.gov/geo/) [19]. All 26 glioma specimens and paired non-tumorous tissues used in this study were collected from glioma patients who underwent the surgical reactions. All the GBM samples were immediately frozen in liquid nitrogen until RNA was extracted.

ceRNA network construction

The differently expressed mRNAs (DEmRNAs), differently expressed lncRNAs (DElncRNAs), and differently expressed miRNAs (DEmiRNAs) in the GSE4290, GSE90603 and GSE104267 datasets were identified by the limma package in R [20]. Differential expression analyses have been carried out with limma setting the FDR threshold to 0.05 and FC lower threshold $|\log(FC)| \geq 1$. We used online tools (http://bioinfogp.cnb.csic.es/tools/venny/) to conduct integrated bioinformatical analyses [21, 22]. MiRcode database (http://www.mircode.org) was used to define the relationships between the DElncRNAs and DEmiRNAs. Target genes were predicted by the miRTarBase, TargetScan, and miRDB. DElncRNA-DEmiRNA-DEmRNA network was constructed by Cytoscape (version3.6.1) [23].

Functional annotation and pathway analysis

We conducted Gene Ontology (GO) enrichment and Kyoto Encyclopedia of Genes and Genome (KEGG) pathway analyses for the mRNAs involved in the constructed lncRNA related network using the R package “clusterprofiler”, with a set of cut-off criteria at $P < 0.05$ [24]. The online database Retrieval of Interacting Gene (STRING) was used to construct Protein-protein interaction (PPI) network [25]. DEmRNAs were incorporated into the PPI network when have a combined score greater than 0.4 [26].

Cell lines and cell culture

All human GBM cell lines (A172, LN229, U87, U251, U373) and normal human astrocyte cell line (NHA) were obtained from the China Infrastructure of Cell Line Resource. Cells were cultured and preserved in DMEM (GIBCO-BRL), which was mixed with 10% FBS, 100 U/mL penicillin and 100 mg/mL streptomycin in a moist air at 37°C with 5% CO_2.

Cell transfection

OXCT1-AS1 inhibitor shRNA and an empty vector were commercially synthesized by General Biology (Anhui, China). The plasmids were transfected at concentration of 2.5μg/well in a 6 well plate. All transfections were finished by using Lipofectamine 2000 (Invitrogen, Carlsbad, CA, USA). The transfection efficiency was assessed by qRT-PCR analysis. Subsequent experiments were performed at 48 h post transfection.

qRT-PCR analysis

Total RNA was extracted from the glioma tissues and cell lines using TRIzol reagent (Ambion, Life Technologies, USA). Reverse transcription was actualized by using a First Strand cDNA Synthesis Kit (TOYOBO Life Science, Shanghai, China). Then, the qRT-PCR analyses were detected using the Universal SYBR-Green Master (Roche, Germany). GAPDH was used as endogenous controls for lncRNAs and mRNAs. U6 was used as endogenous controls for miRNAs. The $2^{-\Delta\Delta Ct}$ method was used for analyzing results.

Cell proliferation assay

The transfection cells were cultured in the 96 well plate at a concentration of 1 × 104 per well and incubated for 24, 48, and 72hr. Cell proliferation was assayed by Cell Counting Kit 8 (CCK-8, MedChem Express, China) according to the manufacturer’s protocol.

Clone formation assay

A density of 5 × 103 cells was planted into 96 well plates. After 24h of transfection with the sh-OXCT1-AS1 and empty vector, cells were seeded into a six well plates (500 per well) and cultured for two weeks. Then, 0.1% crystal violet was used to stain clones, and cells were photographed using a ChemiDocTM MP system (Bio-Rad, USA). The number of colonies was counted using ImageJ.

Cell immunofluorescence staining

After transfection, cells were fixed with 4% paraformaldehyde, permeabilized with Triton X-100 and blocked with 5% bovine serum albumin (BSA, BOSTER, AR0004). Then, cells were incubated with the Ki-67 primary antibody overnight at 4 °C and followed by Alexa Flour 594 AffiniPure goat anti-rabbit IgG (ZSGB-BIO, ZF-0516) as well as DAPI (Beyotime, C1005). The results were determined by the fluorescence microscope in the next day.

Flow cytometry analysis of cell cycling

After transfection, cells were harvested and stained with a CycleTESTTM PLUS DNA Reagent Kit (BD Biosciences). Then, samples were measured by an Accuri C5 flow cytometer (BD Bioscience). The cell cycle results elucidate the exact distribution of the cells in the G0-G1, S, and G2-M phases.

Western blot

The total cell protein was lysed by RIPA buffer (Beyotime Institute of Biotechnology, Beijing, China) with protease and phosphatase inhibitors. The equal amounts of lysates were separated by 12.5% SDS-PAGE gels and transferred to PVDF membranes (Millipore, Billerica, MA). After blocking in 5% skim milk with TBST and incubated with primary antibodies overnight at 4 °C. The membranes were incubated with secondary antibodies at room temperature for 1h. The protein bands were visualized by ChemiDoc^{TM} MP System.

Transwell assay

The 8μm transwell chambers (Corning Company, NY) were used for conducting migration assays. After transfection, cells were planted into the upper chambers (1 × 105 cells/well) and cultured for 24 hr. The chamber was fixed with 4% paraformaldehyde and stained with 0.1% crystal violet for 20~30min. After washing out the crystal violet, stained cells were counted under a microscope. 100μl of Matrigel (BD science, MA) was added into the upper chambers and performed as previously described to detect the cell invasive ability.

Luciferase reporter assay

The fragment of OXCT1-AS1 and CDC25A 3'UTR containing miR-195 binding sites were amplified and cloned to the psiCheck2 reporter vector (Promega, Shanghai, China). Then, HEK293 cells were co-transfected with reporter vector and miR-195 mimics for 48hr. Luciferase activity was measured using Dual Luciferase Reporter Assay (Promega), normalizing firefly (experimental group) luciferase to renilla (control group) activity.

In vivo tumor formation assay

Four weeks old BALB/C nude mice (15-20g) were obtained from the Vital River Animal Center (Beijing, China) randomly divided into two groups. Mice anesthetized with isoflurane were placed in a stereotaxic frame and the skull was exposed for intracranial injections or infusions. After stably transfected with the empty vector or shRNA, LN229 cells were collected and 5×10^6 resuspended cells were used for each intracranial injection. Magnetic resonance imaging was performed to evaluate the intracranial lesions after the vaccinations every 15 days. Tumor volume was assessed and calculated (volume=$(\text{width})^2 \times (\text{length})/2$) every 3 days. The survival time of the mice was recorded and Kaplan-Meier survival curves were plotted for each group.

Immunohistochemistry

Formalin fixed tumor tissues were embedded in paraffin and sliced into 5 μm thick sections. After blocking with 5% BSA, sections were incubated with the CDC25A primary antibody (1:500, Affinity Biosciences, USA) at 4 °C overnight and secondary antibodies at 37°C for 30min. Then, samples were visualized by using the diaminobenzidine (DAB) substrate kit for 10 min. After intensive washing, samples were counterstained with hematoxylin, dehydrated and coverslipped.

Statistical analysis

Data from three independents experiments were shown as the means ± standard deviations (SD). Two groups statistical analysis was performed using Student's t test (two-tailed). For multiple groups statistical analysis, we used one-way ANOVA with SPSS 19.0 (IBM, USA). P-value< 0.05 was considered statistically significant.

Results

Construction of the ceRNA network in GBM

From the GEO database, we downloaded microarray data of GSE4290, which including 23 epileptic tissues and 81 GBM and the microarray data of GSE90603, which including 16 fresh-frozen GBM multiforme samples and 7 healthy brain tissues and the microarray data of GSE104267, including 9 GBM and 3 epileptic tissues. We identified 1292 upregulated mRNAs, and 1709 downregulated mRNAs in GSE4290 (Figure 1A, S1A), 170 upregulated miRNAs and 81 downregulated miRNAs (Figure 1B, S1B) in GSE90603, and 21 upregulated lncRNAs and 69 downregulated lncRNAs (Figure 1C, S1C) in GSE104267, with FC lower threshold |log (FC)|≥1 and P< 0.05. we selected the interaction pairs of lncRNAs and miRNAs based on miRcode database, and the interaction pairs of miRNAs and mRNAs based on the miRDB database, TargetScan and miRTarBase. We constructed a lncRNA-miRNA-mRNA competing network. Finally, a total of 12 DElncRNAs, 3 DEmiRNAs, and 116 DEmRNAs were employed to construct the ceRNA network using Cytoscape, as shown in Figure 1D. We found lncRNA OXCT1-AS1 have a connection with two of the three DEmiRNAs and therefore we focused on OXCT1-AS1 in the following experiments. According to the ceRNA network hypothesis, we found that expression of OXCT1-AS1 was only conversely related to miR-195 level. Hence, we hypothesized that mir-195 might be the downstream target of OXCT1-AS1 in the ceRNA network.

GO functional annotation and the KEGG pathway enrichment analysis

We Used the ClusterProfile package in R software to perform the GO functional enrichment and the KEGG pathway enrichment analyses. GO analysis showed that the DEmRNAs we obtained were associated with "cell cycle," "membrane enclosed lumen," "transcription factor activity," and so on (Figure 2, Table S1-S3). KEGG pathway analysis showed that the DEmRNAs were enriched in cancer associated pathways, such as MicroRNA in cancer, cell cycle and so on (Figure 2, Table 1). Both GO and KEGG analysis all enriched in cell cycle process. From the ceRNA network, we searched the cell cycle related DEmRNAs can be regulated by miR-195 and found cell division cycle 25A (CDC25A) was the only candidate. We also used the STRING database to explore the hub genes from the DEmRNAs and constructed the PPI network (Figure 2). We identified the top 10 DEmRNAs as the hub genes based on their linkage degree, including CDC25A (Figure 2). Thus, CDC25A might be the component of OXCT1-AS1/miR-195 axis regulated ceRNA network.

Table 1 KEGG cell signaling pathway analysis of DEmRNAs in lncRNA related ceRNA networks.

ID	Description	Adjusted P values	Counts	Gene names
hsa05206	MicroRNAs in cancer	0.00000602	9	MCL1/CDC25A/NOTCH2/BCL2L2/VEGFA/CDKN1A/KIF23/SOX4/TIMP3
hsa04110	Cell cycle	0.0000297	6	CDC25A/WEE1/CHEK1/CDKN1A/E2F5/YWHAH
hsa01522	Endocrine resistance	0.00011607	5	NCOA3/CDKN1A/MAPK9/JAG1/NOTCH2
hsa04114	Oocyte meiosis	0.00027439	5	PPP3R1/BTRC/ITPR1/YWHAH/CPEB3
hsa05200	Pathways in cancer	0.00056634	8	RASGRP1/RUNX1T1/VEGFA/CDKN1A/GNB5/HIF1A/MAPK9/LAMC1
hsa04010	MAPK signaling pathway	0.00132625	6	PPP3R1/RASGRP1/DUSP2/MAP3K1/MAPK9/MEF2C
hsa05202	Transcriptional misregulation in cancer	0.00157405	5	CDKN1A/RUNX1T1/MEF2C/HOXA10/PBX3
hsa05205	Proteoglycans in cancer	0.0029711	5	CDKN1A/ITPR1/TIMP3/VEGFA/HIF1A
hsa04115	p53 signaling pathway	0.00438531	3	CDKN1A/CHEK1/RRM2
hsa04151	PI3K-Akt signaling pathway	0.00536491	6	VEGFA/MCL1/CDKN1A/GNB5/YWHAH/LAMC1
hsa04921	Oxytocin signaling pathway	0.00681985	4	CDKN1A/PPP3R1/ITPR1/MEF2C
hsa05166	HTLV-I infection	0.00730939	5	CDKN1A/PPP3R1/MAP3K1/CHEK1/TP53INP1
hsa04320	Dorso-ventral axis formation	0.00825292	2	CPEB3/NOTCH2
hsa04710	Circadian rhythm	0.00935463	2	BTRC/CRY2
hsa04912	GnRH signaling pathway	0.00943716	3	MAP3K1/ITPR1/MAPK9
hsa04914	Progesterone mediated oocyte maturation	0.0108457	3	MAPK9/CPEB3/CDC25A
hsa04723	Retrograde endocannabinoid signaling	0.01205547	3	ITPR1/MAPK9/GNB5
hsa04066	HIF-1 signaling pathway	0.01333979	3	CDKN1A/HIF1A/VEGFA
hsa04660	T cell receptor signaling pathway	0.01401011	3	PPP3R1/RASGRP1/MAPK9
hsa05219	Bladder cancer	0.01648587	2	CDKN1A/VEGFA
hsa04724	Glutamatergic synapse	0.01688062	3	PPP3R1/ITPR1/GNB5
hsa04919	Thyroid hormone signaling pathway	0.01923358	3	NCOA3/HIF1A/NOTCH2
hsa04330	Notch signaling pathway	0.02190805	2	JAG1/NOTCH2
hsa04728	Dopaminergic synapse	0.0226392	3	ITPR1/MAPK9/GNB5

hsa04014	Ras signaling pathway	0.0227743	4	RASGRP1/VEGFA/MAPK9/GNB5
hsa04380	Osteoclast differentiation	0.02445721	3	PPP3R1/OSCAR/MAPK9
hsa04068	FoxO signaling pathway	0.02539501	3	CDKN1A/GABARAPL1/MAPK9
hsa04210	Apoptosis	0.02882821	3	MAPK9/ITPR1/MCL1
hsa04310	Wnt signaling pathway	0.02882821	3	PPP3R1/BTRC/MAPK9
hsa05161	Hepatitis B	0.03195714	3	CDKN1A/MAP3K1/MAPK9
hsa04370	VEGF signaling pathway	0.03660229	2	PPP3R1/VEGFA
hsa04924	Renin secretion	0.03660229	2	PPP3R1/ITPR1
hsa05131	Shigellosis	0.03864514	2	BTRC/MAPK9
hsa04720	Long-term potentiation	0.03864514	2	PPP3R1/ITPR1
hsa05212	Pancreatic cancer	0.04073055	2	VEGFA/MAPK9
hsa05211	Renal cell carcinoma	0.04178893	2	HIF1A/VEGFA
hsa04622	RIG-I-like receptor signaling pathway	0.0428576	2	MAP3K1/MAPK9
hsa04141	Protein processing in endoplasmic reticulum	0.0429848	3	MAPK9/TRAM1/PDIA6
hsa04022	cGMP-PKG signaling pathway	0.04681452	3	PPP3R1/ITPR1/MEF2C
hsa04260	Cardiac muscle contraction	0.04835144	2	TPM2/SLC9A6

LncRNA OXCT1-AS1 was highly expressed in GBM and associated with prognosis

We first examined the expression pattern of lncRNA OXCT1-AS1 in various types of common solid cancers based on the results from TCGA database analysis and found OXCT1-AS1 was aberrantly expressed in GBM and low-grade glioma (LGG) as shown in figure 3A. In the GBM, the patients with high OXCT1-AS1 expression have a lower median survival of 37.75 months compared with the low OXCT1-AS1 expression group of 53.52 months. The overall survival status significantly differed between the high OXCT1-AS1 expression group and the low OXCT1-AS1 expression group (HR= 1.52, 95% CI 1.094-2.163, *P* value= 0.0132; Figure 3B). We also analyzed 26 pairs of GBM samples and their adjacent normal tissues, the expression of OXCT1-AS1 remarkably increased in the GBM samples (Figure 3C). Kaplan-Meier analysis was used to evaluate the OXCT1-AS1 related patient survival and the result showed that higher OXCT1-AS1 expression with the poor survival (HR=1.922, 95% CI 1.154-3.203, *P* value=0.0245; Figure 3E). Could OXCT1-AS1 be an indicator for the diagnosis of GBM? We used the 26 paired adjacent normal tissues as controls to build the ROC curve (Figure 3D). The sensitivity and specificity were 0.769 and 0.808, respectively. The cutoff value was 1.1545. The area under the curve was 0.817 (95% CI=0.692–0.941, P< 0.000). The Youden index was 0.577. In the univariable and multivariable Cox regression model, we found that the OXCT1-AS1 expression can be an indicator of GBM (HR=0.468 95% CI 0.094-0.361, *P* value=0.014; Table 2). The qRT-PCR assays also demonstrated that CDC25A was downregulated in glioma tissues (Figure 3F), which was opposite to miR-195 but was consistent with OXCT1-AS1 (Figure 3G-I).

Table 2 Univariable and multivariable Cox regression analysis in GBM

Characteristics	Subset	Univariate analysis Hazard ratio(95%CI)	P value	Univariate analysis Hazard ratio(95%CI)	P value
Age	≤48/>48	1.378(0.451-4.214)	0.751	1.794(0.243-4.241)	0.981
Gender	Male/Female	1.556(0.643-3.749)	0.327	3.165(0.981-10.210)	0.885
Chr7 gain/Chr10 loss	Yes/No	0.318(0.126-0.804)	0.015*	0.908(0.246-3.358)	0.054
1p/19q status	Code/Noncoded	9.036(7.841-37.803)	0.000*	4.355(1.121-16.443)	0.002*
IDH status	Mutation/Wild	0.630(2.701-3.242)	0.003*	0.170(0.042-0.691)	0.013*
MGMT promoter status	Mutation/Wild	7.151(3.606-81.581)	0.011*	5.706(1.986-34.619)	0.064
OXCT1-AS1	High/Low	0.701(0.191-0.541)	0.000*	0.468(0.094-0.361)	0.014*

In both univariable and multivariable Cox regression analyses, all characteristics were evaluated as continuous variables. $P < 0.05$ was considered statistically significant in all analyses.

LncRNA OXCT1-AS1 has a higher expression level in GBM cell lines and suppression of OXCT1-AS1 can arrest GBM cells proliferation

We performed the qRT-PCR assays to test the OXCT1-AS1 expression level in GBM cell lines and the result showed that the expression levels of OXCT1-AS1 were upregulated in GBM cells compared with NHA cells (Figure 4A). As A172 and LN229 have the highest expression of OXCT1-AS1 among the GBM cell lines, so we selected them for this study. We transfected shRNA in A172 and LN229 cells to suppress the OXCT1-AS1 expression. After 48h post-transfection, qRT-PCR analysis was performed and the result showed that the 1st and 2nd shRNA significantly downregulated OXCT1-AS1 expression (Figure 4B). We selected the 1st shRNA for further experiments. The CCK-8 assay result showed that the viability of A172 and LN229 cells was obviously decreased by shRNA transfection (Figure 4C, F). Similarly, depressed OXCT1-AS1 expression impaired the colony formation capacities of GBM cells (Figure 4D, E). At last, we used Ki-67 staining assays to measure cell proliferation. The proliferative marker Ki67 was decreased after OXCT1-AS1 knockdown (Figure 4G, H).

LncRNA OXCT1-AS1 promotes the migration and invasion of GBM cells in vitro

We also studied whether OXCT1-AS1 could affect the migration and invasion of GBM cells. The cell migration and invasion potential were measured by the Transwell assays. Respectively, the results showed both the migration and invasion cells were significantly decreased after silencing OXCT1-AS1 (Figure 5A-D). Additionally, the expression levels of the related proteins were measured. As presented in Figure 5E and 5F, knocking down of OXCT1-AS1 increased the protein level of E-cadherin, while decreased the protein levels of N-cadherin and snail, further confirmed our Transwell results.

Depression of OXCT1-AS1 induced cell cycle arrest in GBM cells

As our KEGG pathway enrichment analyses has point out the obtained hub genes may regulate cell cycle process. So, we conducted flow cytometry assays to evaluate the impact of OXCT1-AS1 on the GBM cell cycle. After silencing OXCT1-AS1 in GBM cells, the quantity of cells in the G0/G1 phase was increased and the amount of cells in the G2/M phase was decreased (Figure 6A-D), confirming that OXCT1-AS1 promotes GBM malignant progression, might partly by regulating cell cycle process. Additionally, through constructing ceRNA network, we found OXCT1-AS1 may influence GBM cell cycle by regulating CDC25A. Furthermore, we measured the levels of proteins associated with cell cycle as CDC25A, CCNA1, CCNE1 and CDK2 (the downstream tyrosine dephosphorylating target of CDC25A). As presented in Figure 5E, knocking down of OXCT1-AS1 can significantly decrease the protein levels of CDC25A, CCNA1, CCNE1 and upregulate CDK2 phosphorylation levels (Figure 5F). All these experiments further proved our conjecture.

OXCT1-AS1 enhanced the expression level of CDC25A by competitively binding miR-195 in GBM cells

At the beginning, we have conducted microarray analysis and constructed the ceRNA network to explore the underlying molecular mechanism of OXCT1-AS1. To examine whether OXCT1-AS1 function as a ceRNA in GBM cells, we used online software LncBase V2.0 (http://carolina.imis.athena-innovation.gr) to predict the binding sit of OXCT1-AS1 and miR-195, the result was shown in Figure 7A and the qRT-PCR assay showed that knocking down of OXCT1-AS1 can increase the level of miR-195 in GBM cells (Figure 7B). To confirm the competing sponging mechanism, we constructed wild type and mutant type (mut) of OXCT1-AS1 luciferase reporter separately with psiCheck2 vector. According to the results of dual luciferase reporter assay, the results realized that miR-195 mimics can reduce the luciferase activity of wild type OXCT1-AS1 reporter, but no significant change was observed in the OXCT1-AS1 mutant reporter (Figure

7D). All these results demonstrated OXCT1-AS1 direct targeted miR-195 and the expression of the latter was inhibited. Based on our previous microarray analysis result, CDC25A predicted as the downstream of the miR-195 in the ceRNA network. The binding sequence between miR-195 and CDC25A was predicted and exhibited in Figure 7C. Similarly, the luciferase activity of the wild type CDC25A but not that of mutant type CDC25A was reduced by miR-195 mimics (Figure 7E). We also conducted the western blot assay and the results indicated that the expression of CDC25A was decreased in the OXCT1-AS1 knockdown group compared with the vector group, whereas the inhibiting effect could be partially reversed by adding miR-195 inhibitor AMO-195 (Figure 7F). Functional experiment by clone formation assay also revealed miR-195 inhibitor can partly reverse the OXCT1-AS1 knockdown induced GBM cell growth arrest (Figure 7G). In summary, OXCT1-AS1 can promote GBM cells proliferation by competitively binding miR-195 and negatively regulating the miR-195/ CDC25A axis.

Knocking down of OXCT1-AS1 inhibited GBM cell tumorigenesis in vivo

To investigate the impact of OXCT1-AS1 in tumorigenesis, the vivo experiment was conducted. As showed in Figure 8A and 8B, primary GBM cells derived mouse intracranial tumors were obvious smaller after knocking down of OXCT1-AS1 than those derived from cells transfected with empty vector. Consistently, the survival time in OXCT1-AS1 silencing group was longer than those in vector group (Figure 8C). Then, qRT-PCR experiment determined an obvious increase in miR-195 expression in the tumor tissue derived from sh-OXCT1-AS1 transfected cells (Figure 8D). Through immunohistochemistry assay, we found the expression level of CDC25A was decreased in OXCT1-AS1 blocking group compared with vector group (Figure 8F). All these findings indicated that OXCT1-AS1 can promote GBM cell tumorigenesis in vivo.

Discussion

Since lacking of effective therapeutic targets, patients with GBM usually have the worst survival rate [7, 27]. It's urgently to identify new, suitable and effective therapeutic targets [28]. In recent studies, deregulation of lncRNA has been revealed in various malignancies and implicates potential biomarker and therapeutic targets [29-31]. For instance, lncRNA LINC00899 suppresses breast cancer progression by inhibiting miR-425 [32], lncRNA ZFAS1 regulates esophageal squamous cell carcinoma cell malignant behaviors via miR-124/STAT3 axis [33] and lncRNA MALAT1 promotes GBM proliferation and progression by targeting miR-199a/ZHX1 axis [34]. All these studies have indicated that lncRNAs play an important role in the diagnose and treatment of human cancers. In our present study, we identified DElncRNAs, DEmiRNAs and DEmRNAs in GBM and normal brain samples from the GEO databases. We further constructed a putative ceRNA network and preformed GO and KEGG pathway enrichment analysis. From the ceRNA network, we identified the core lncRNA OXCT1-AS1. In our subsequent studies, we focused on verifying OXCT1-AS1 can be the specific biomarker and potent therapeutic target for GBM. We identified that the lncRNA OXCT1-AS1 was aberrantly expressed in GBM tissue and the raised of OXCT1-AS1 expression was associated with poor overall survival. This result was confirmed in vitro experiment, the blocking of OXCT1-AS1 can efficiently suppress cell proliferation, induce cell cycle arrest and inhibit migration and invasion of GBM cells. In vivo experiments, we demonstrated that knocking down of OXCT1-AS1 can inhibited GBM cell tumorigenesis. Collectively, our data demonstrated that OXCT1-AS1 acting as a oncogene in GBM and have the potential to become a specific diagnostic and prognostic biomarker as well as a therapeutic target in GBM.

To further investigate the potential mechanisms, we filtered the down regulated DEmiRNA from the ceRNA network we constructed. Based on the ceRNA network hypothesis, we conducted bioinformatics analysis using LncBase V2.0, the results showed that OXCT1-AS1 contained a conserved target site of miR-195. Previous studies have proved that miR-195 can act as a tumor suppressor in various cancers [35-37]. In our study, we explored the potential targets of miR-195. According to the result of KEGG enrichment analysis, we screened the DEmRNA matched with cell cycle pathway and used TargetScan to predict the conserved target site. We found CDC25A can be the direct target of miR-195. The CDC25A is a member of CDC25 phosphatase family and plays important role in cell cycle regulation by activating of cyclins-CDKs through removal of the inhibitory phosphates [38]. Ectopic expression of CDC25A accelerates the G1/S phase transition [39, 40]. In our research, knocking down of OXCT1-AS1 can reduce the expression level of CDC25A and increase the CDK2 phosphorylation levels. Flow cytometry assays also confirmed that knocking down of OXCT1-AS1 caused cell cycle arrest. Further luciferase activity assays and functional experiments demonstrated that OXCT1-AS1 can promote GBM proliferation by acting as a ceRNA and regulate the miR-195/ CDC25A axis.

Conclusions

This study, we first identified lncRNA OXCT1-AS1 as the potential predictor and therapeutic target of GBM. Knocking down of OXCT1-AS1 significantly inhibited proliferation, migration, invasion and tumorigenesis in GBM. We also investigated the molecular mechanism

involved and demonstrated that OXCT1-AS1 might act as a ceRNA and regulate miR-195/ CDC25A axis. Our findings provided a novel regulatory network in GBM, which can help us look insight of the pathogenesis of GBM and improve the treatment for GBM patients.

Abbreviations

lncRNAs: long noncoding RNAs; GBM: glioblastoma; ceRNA: competing endogenous RNA network; OXCT1-AS1: OXCT1 antisense RNA 1; GEO: Gene Expression Omnibus; TCGA: The Cancer Genome Atlas; qRT-PCR: quantitative real-time PCR; DEmRNAs: differently expressed mRNAs; DEmiRNAs: differently expressed miRNAs; DElncRNAs: differently expressed lncRNAs; GO: Gene Ontology; KEGG: Kyoto Encyclopedia of Genes and Genome; PPI: Protein-protein interaction; STRING: Search Tool for the Retrieval of Interacting Gene; CDC25A: cell division cycle 25A.

Declarations

Acknowledgements

We thank Yan Tao for the excellent technical assistance.

Funding

This work was supported by China Postdoctoral Science Foundation (grant No.2020M681888), National Key R&D program of China (grant No.2018YFC1312600; 2018YFC1312603), the Key Research and Development Project of Zhejiang Province (grant No.2018C03011) and TCM Key Discipline of Zhejiang province (grant No.2017-XK-A39).

Availability of data and material

Due to our internal policy, raw data cannot be shared.

Author Contributions

ZC mainly conceived, performed this experiment and also wrote the paper, L Z-D helped analyzed the microarray data, Z S-G collected the clinical samples, YQ, Z S-J and P Y-C helped with the experiments, YD and G L-G performed the statistical analysis in this study. CG carried out the experiment design and manuscript drafting. All authors had edit and approved the final manuscript.

Ethics approval and consent to participate

All experimental ethics and animal experiments were conformed to the European Parliament Directive (2010/63/EU) and were approved by the Institutional Animal Care and Use Committee at Harbin Medical University (No. HMUIRB-2008-06).

Consent for publication

Not applicable.

Competing interests

The authors declared no potential conflicts of interest with respect to the research, authorship, and/or publication of this article.

References

1. Mary D. Glioblastoma: Overview of Disease and Treatment. Clinical Journal of Oncology Nursing. 2016; 20(5 Suppl):S2-S8.
2. Brandner S, Jaunmuktane Z. Neurological update: gliomas and other primary brain tumours in adults. J Neurol. 2018;265(3):717-727.
3. Chen R, Smith-Cohn M, Cohen AL, Colman H. Glioma Subclassifications and Their Clinical Significance. Neurotherapeutics. 2017;14(2):1-14.
4. Alan O, Telli TA, Tuylu TB, Arikan R, Demircan NC, Ercelep O, et al. Prognostic factors in progressive high-grade glial tumors treated with systemic approach: A single center experience. Journal of Oncology Pharmacy Practice. 2020;0(0):1078155220920684.

5. Jiang HH, Lin S. Current status and prospect in the treatment of glioblastoma. Zhonghua wai ke za zhi Chinese journal of surgery. 2020;58(1):70-4.
6. Chen R S-CM, Cohen AL, Colman H. Molecular profiling of gliomas: Potential therapeutic implications. Expert Review of Anticancer Therapy. 2015;15(8):955-62.
7. Zhou L, Tang H, Wang F, Chen L, Ou S, Wu T, et al. Bioinformatics analyses of significant genes, related pathways and candidate prognostic biomarkers in glioblastoma. Mol Med Rep. 2018;18(5):4185-96.
8. Dragomir MP, Kopetz S, Ajani JA, Calin GA. Non-coding RNAs in GI cancers: From cancer hallmarks to clinical utility. Gut. 2020;69(4):748-763.
9. Grillone K, Riillo C, Scionti F, Rocca R, Tassone P. Non-coding RNAs in cancer: platforms and strategies for investigating the genomic "dark matter". Journal of Experimental & Clinical Cancer Research. 2020;39(1):117.
10. Liao Y, Jung SH, Kim T. A-to-I RNA editing as a tuner of noncoding RNAs in cancer. Cancer Letters. 2020;494:88-93.
11. Costa FF. Non-coding RNAs: Meet thy masters. Bioessays. 2010;32(7):599-608.
12. A RC, A MJS, A ALH, B RSA, C KYL, A EIR, et al. Long noncoding RNAs in cancer: From discovery to therapeutic targets. Advances in Clinical Chemistry. 2020;95:105-47.
13. Zhang X-Z, Liu H, Chen S-R. Mechanisms of Long Non-Coding RNAs in Cancers and Their Dynamic Regulations. Cancers. 2020;12:1245.
14. Peng Z, Liu C, Wu M. New insights into long noncoding RNAs and their roles in glioma. Molecular Cancer. 2018;17(1):61.
15. Guzel E, Okyay TM, Yalcinkaya B, Karacaoglu S, Gocmen M, Akcakuyu MH. Tumor suppressor and oncogenic role of long non-coding RNAs in cancer. Northern Clinics of Istanbul. 2019;7(1):81-86.
16. Tay Y, Rinn J, Pandolfi PP. The multilayered complexity of ceRNA crosstalk and competition. Nature. 2014;505(7483):344-52.
17. Ala U. Competing Endogenous RNAs, Non-Coding RNAs and Diseases: An Intertwined Story. Cells. 2020;9(7):1574.
18. Sun L, Hui AM, Su Q, Vortmeyer A, Kotliarov Y, Pastorino S, et al. Neuronal and glioma-derived stem cell factor induces angiogenesis within the brain. Cancer Cell. 2006;9(4):287-300.
19. Gulluoglu S TE, Sahin M, Kuskucu A, Kaan Yaltirik C, Ture U, Kucukkaraduman B, Akbar MW, Gure AO, Bayrak OF, Dalan AB. Simultaneous miRNA and mRNA Transcriptome Profiling of Glioblastoma Samples Reveals a Novel Set of OncomiR Candidates and Their Target Genes. Brain Research. 2018;1700:199-210.
20. Feng F, Wu J, Gao Z, Yu S, Cui Y. Screening the key microRNAs and transcription factors in prostate cancer based on microRNA functional synergistic relationships. Medicine (Baltimore). 2017;96(1):e5679.
21. Zhang J, Zhou YJ, Yu ZH, Chen AX, Cao XC. Identification of core genes and clinical roles in pregnancy-associated breast cancer based on integrated analysis of different microarray profile datasets. Bioence Reports. 2019;39(6): BSR20190019.
22. Anders S, Huber W. Differential expression analysis for sequence count data. Genome Biology. 2010;11(10):R106.
23. Cline MS, Smoot M, Cerami E, Kuchinsky A, Landys N, Workman C, et al. Integration of biological networks and gene expression data using Cytoscape. Nature Protocols. 2007;2(10):2366-2382.
24. Yin J, Zeng X, Ai Z, Yu M, Wu Yo, Li S. Construction and analysis of the lncRNA-miRNA-mRNA network based on competitive endogenous RNA reveal functional lncRNAs in oral cancer. BMC Med Genomics. 2020;13(1):84.
25. von Mering C HM, Jaeggi D, Schmidt S, Bork P, Snel B. STRING: a database of predicted functional associations between proteins. Nucleic Acids Res. 2003;31(1):258-61.
26. Yi F, Sun M, Dai G, Ramani K. The Intrinsic Geometric Structure of Protein-Protein Interaction Networks for Protein Interaction Prediction. IEEE/ACM Trans Comput Biol Bioinform. 2016;13(1):76-85.
27. Ana, Miranda, María, Blanco-Prieto, João, Sousa, et al. Breaching barriers in glioblastoma. Part I: Molecular pathways and novel treatment approaches. International Journal of Pharmaceutics. 2017;531(1):372-388.
28. Taylor OG, Brzozowski JS, Skelding KA. Glioblastoma Multiforme: An Overview of Emerging Therapeutic Targets. Frontiers in Oncology. 2019;9:963.
29. Athina, Kladi-Skandali, Kleita, Michaelidou, Andreas, Scorilas, et al. Long Noncoding RNAs in Digestive System Malignancies: A Novel Class of Cancer Biomarkers and Therapeutic Targets? Gastroenterology Research & Practice. 2015;2015:319861.
30. Fatima R, Akhade VS, Pal D, Rao SM. Long noncoding RNAs in development and cancer: potential biomarkers and therapeutic targets. Molecular & Cellular Therapies. 2015;3(1):5.

31. Wang L, Cho KB, Li Y, Tao G, Guo B. Long Noncoding RNA (lncRNA)-Mediated Competing Endogenous RNA Networks Provide Novel Potential Biomarkers and Therapeutic Targets for Colorectal Cancer. International Journal of Molecular Ences. 2019;20(22):5758.
32. Zhou W, Gong J, Chen Y, Chen J, Zhuang Q, Cao J, et al. Long noncoding RNA LINC00899 suppresses breast cancer progression by inhibiting miR-425. Aging (Albany NY). 2019;11(22) :10144-10153.
33. Li Z, Qin X, Bian W, Li Y, Li S. Exosomal lncRNA ZFAS1 regulates esophageal squamous cell carcinoma cell proliferation, invasion, migration and apoptosis via microRNA-124/STAT3 axis. Journal of Experimental & Clinical Cancer Research. 2019;38(1) :477.
34. Liao K, Lin Y, Gao W, Xiao Z, Guo L. Blocking lncRNA MALAT1/miR-199a/ZHX1 axis inhibits glioblastoma proliferation and progression. Mol Ther Nucleic Acids. 2019;18:388-399.
35. Jin M, Wang L, Zheng T, Yu J, Sheng R, Zhu H. MiR-195-3p inhibits cell proliferation in cervical cancer by targeting BCDIN3D. Journal of Reproductive Immunology. 2020;143:103211.
36. Liu X, Zhou Y, Ning YE, Gu H, Tong Y, Wang N. MiR-195-5p Inhibits Malignant Progression of Cervical Cancer by Targeting YAP1. Oncotargets & Therapy. 2020;13 :931-944.
37. Long Z, Wang Y. miR-195-5p Suppresses Lung Cancer Cell Proliferation, Migration, and Invasion Via FOXK1. Technology in Cancer Research Treatment. 2020;19 :1533033820922587.
38. Sadeghi H, Golalipour M, Yamchi A, Farazmandfar T, Shahbazi M. CDC25A pathway toward tumorigenesis: Molecular targets of CDC25A in cell-cycle regulation. J Cell Biochem. 2019;120(3):2919-2928.
39. Blomberg I, Hoffmann I. Ectopic Expression of Cdc25A Accelerates the G1/S Transition and Leads to Premature Activation of Cyclin E- and Cyclin A-Dependent Kinases. Molecular & Cellular Biology. 1999;19(9):6183-94.
40. Kabakci Z, Käppeli S, Cantù C, Jensen LD, König C, Toggweiler J, et al. Pharmacophore-guided discovery of CDC25 inhibitors causing cell cycle arrest and tumor regression. Scientific Reports. 2019;9(1):1335.

Figures

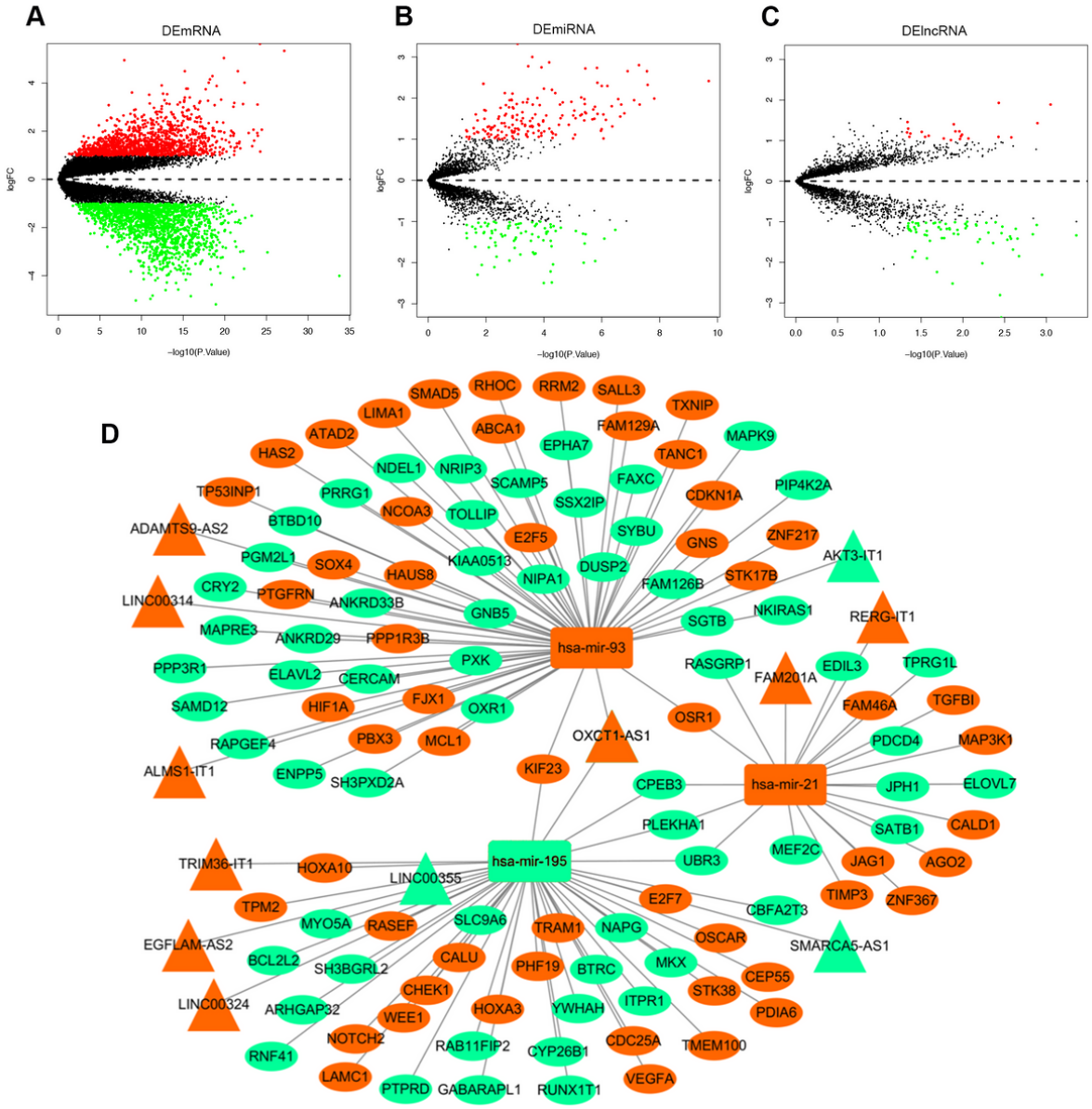

Figure 1

Expression distribution of differential lncRNAs, miRNAs and mRNAs. (A) Different expressed mRNAs from GSE4290. (B) Different expressed miRNAs from GSE104267. (C) Different expressed mRNAs from GSE90603. The red plots in the plot represent the up regulated targets with statistical significance and the green plots represent the down regulated targets with statistical significance. (D) The ceRNA network in GBM. Red nodes represent upregulated different expressed RNAs and green nodes represent downregulated different expressed RNAs. DElncRNAs, DEmiRNAs, and DEmRNAs are represented by triangles, rectangles, and ellipses, respectively.

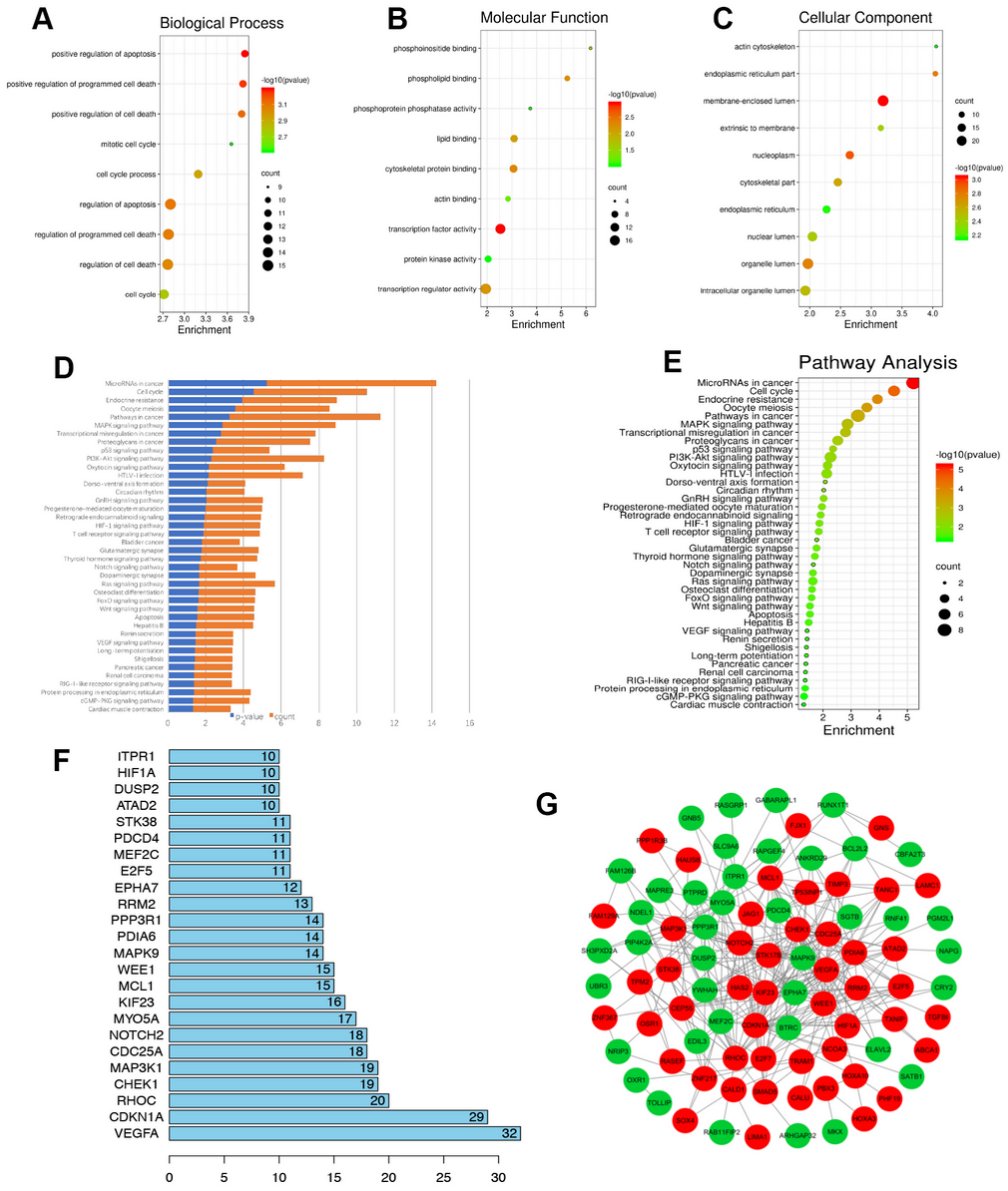

Figure 2

GO functional annotation and the KEGG pathway enrichment analysis and the hub genes involved in these pathways. (A) GO functional enrichment in cell biological process. (B) GO functional enrichment in cell molecular function. (C) GO functional enrichment in cellular function. (D, E) KEGG cell signal pathway enrichment of the ceRNA network. (F) the hub genes with high degree of connectivity between DEmRNAs. (G) PPI network of DEmRNAs we obtained from the ceRNA network. Red nodes represent upregulated DEmRNAs and green nodes represent downregulated DEmRNAs. PPI, protein-protein interaction.

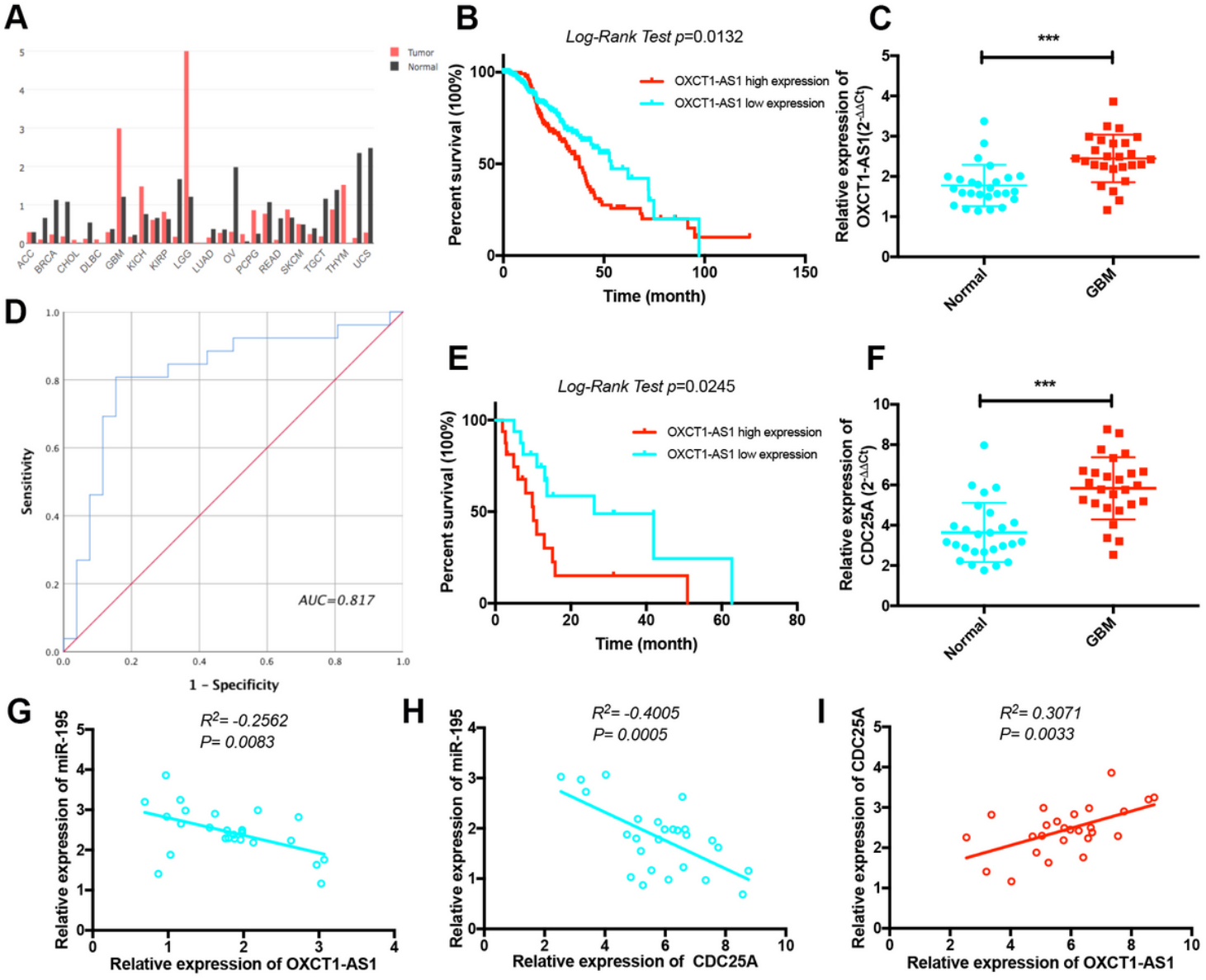

Figure 3

LncRNA OXCT1-AS1 was highly expressed in GBM and associated with prognosis. (A) The OXCT1-AS1 expression patterns in different types of solid cancers from TCGA database. (B) Kaplan-Meier curve analysis of the OXCT1-AS1 based on TCGA GBM samples. (C) The expression of OXCT1-AS1 was examined by qRT-PCR in GBM tissues compared with corresponding adjacent normal tissues. (D) The ROC curve was constructed using SPSS. The area under the curve was 0.817. The sensitivity and specify were 0.769 and 0.808, respectively. (E) the survival time of GBM patients was longer in the OXCT1-AS1 low expression group than the high expression group. (F) The expression of CDC25A was examined by qRT-PCR in GBM tissues compared with corresponding adjacent normal tissues. (G) The negative expression correlation between OXCT1-AS1 and miR-195 in GBM tissues was analysis. (H) The correlation between the expression of miR-195 and CDC25A. (I) the positive expression correlation between OXCT1-AS1 and CDC25A. (The statistic bars represent SD, *p<0.05, **p<0.01, ***p<0.001).

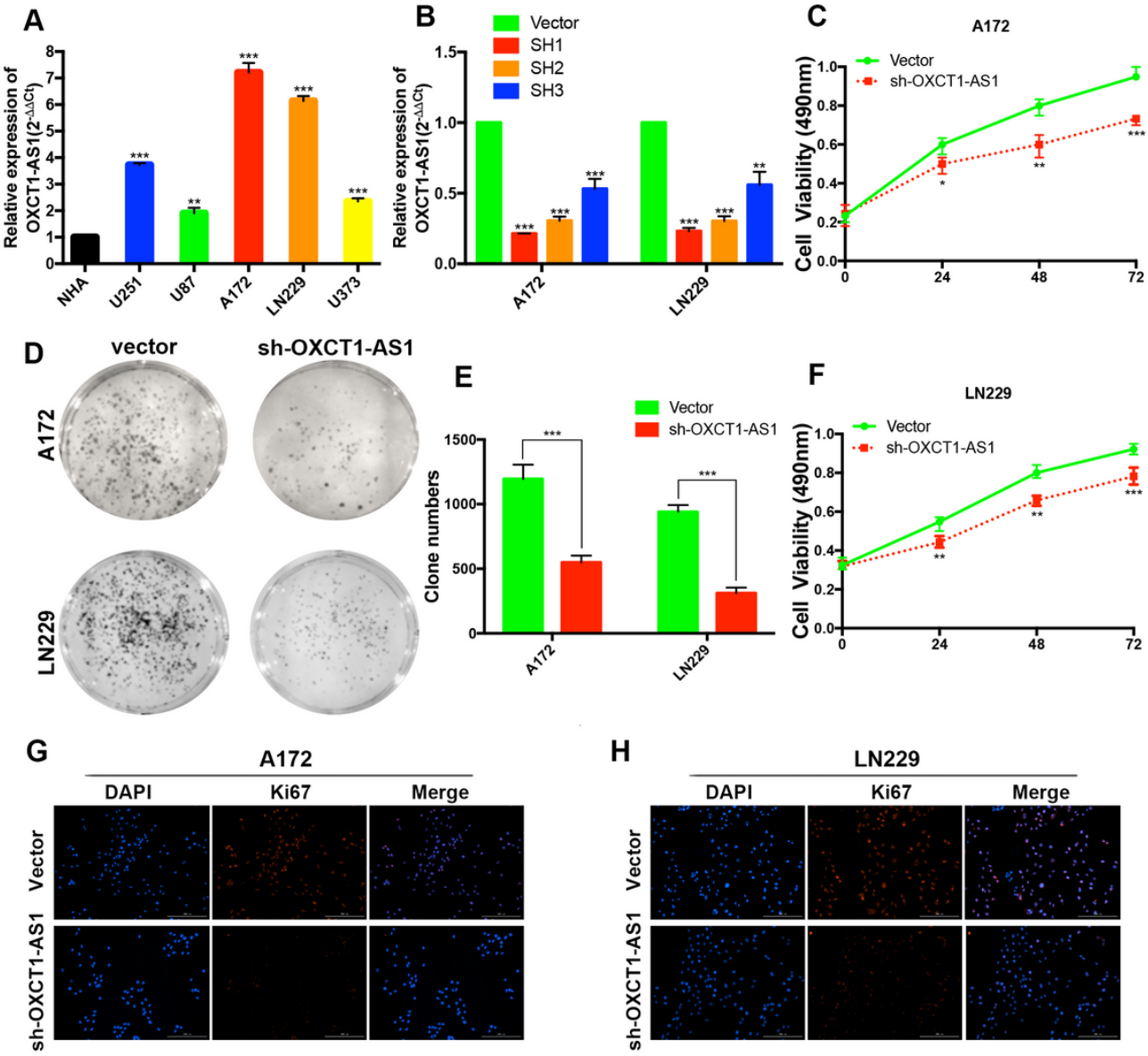

Figure 4

Knocking down of OXCT1-AS1 markedly suppressed the proliferation of GBM cells in vivo. (A) OXCT1-AS1 expression levels in GBM cell lines compared with human brain astrocyte cell line NHA. (B) 3 shRNA of OXCT1-AS1 and the empty vector were transfected into A172 and LN229 cells. The inhibitory efficiency was measured by the qRT-PCR assay. (C, F) After transfecting sh-OXCT1-AS1 and vector, CCK8 cell proliferation assays were performed at 0, 24, 48, 72hr. (D, E) colony formation assays performed with the A172 and LN229 cells transfected with sh-OXCT1-AS1 and vector. (G, H) Fluorescence microscopy of Ki67 expression after silencing of OXCT1-AS1 or transfected with the empty vector. The scale bar represents 100 μm. The bars represent SD (*p<0.05, **p<0.01, ***p<0.001).

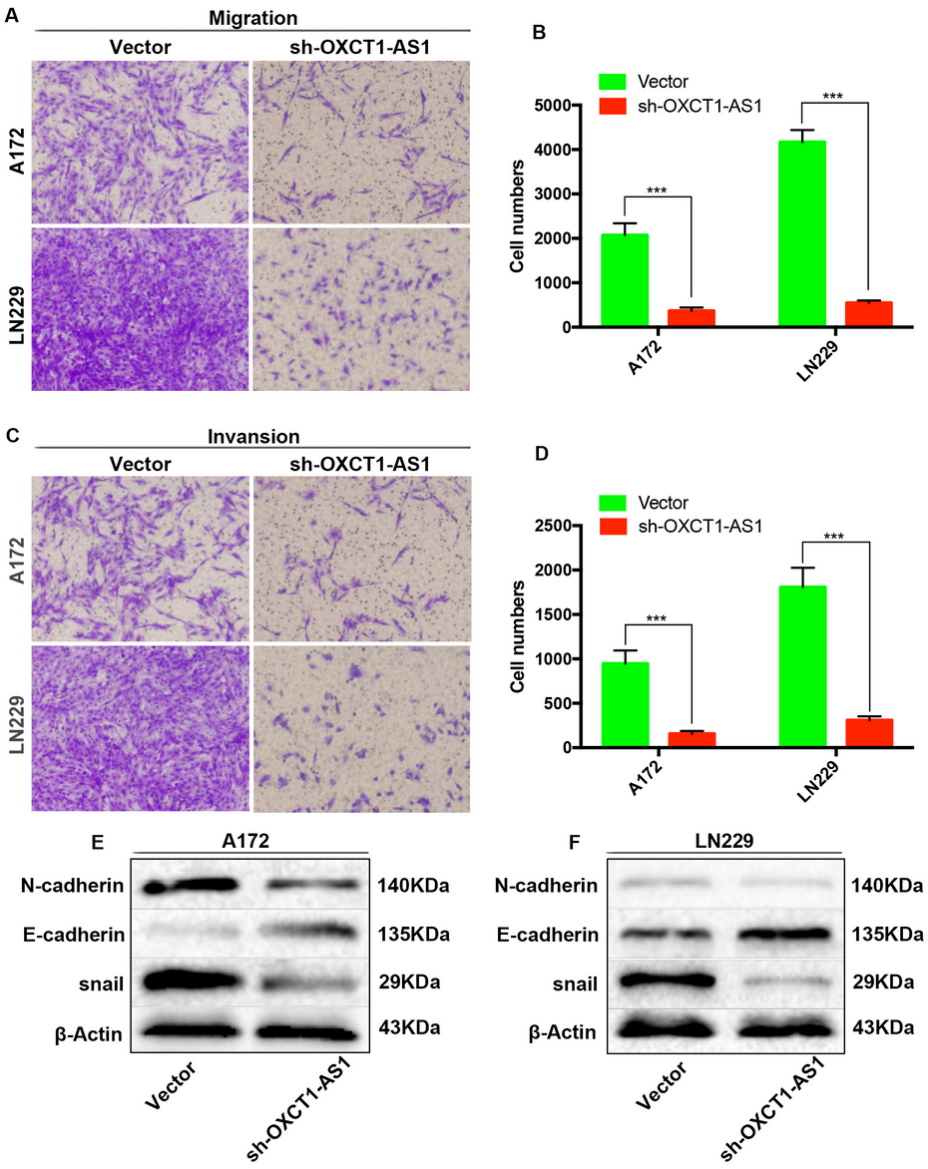

Figure 5

OXCT1-AS1can promote the migration and invasion of GBM cells in vitro. (A, B) Transwell assay were performed to detect the migrative ability in A172 and LN229 cell lines transfected with sh-OXCT1-AS1 and vector. (C, D) the invasive ability were measured by Transwell assay with Matrigel in A172 and LN229 cell lines transfected with sh-OXCT1-AS1 or vector. (E, F) After transfecting with sh-OXCT1-AS1 and vector, the migration and invasion related proteins as N-cadherin, E-cadherin and snail were examined by western blot assay. β-Actin was used as the internal control.

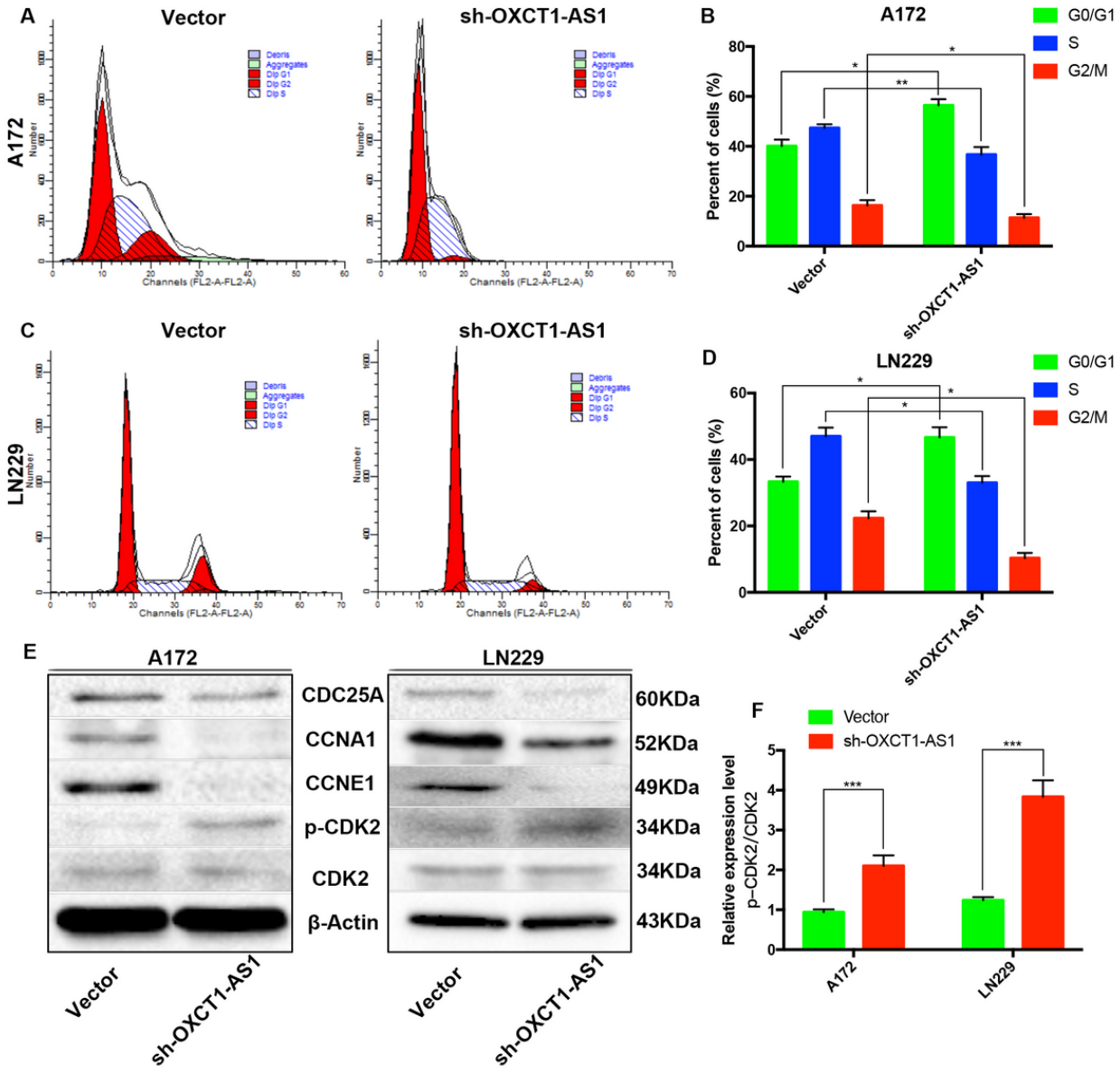

Figure 6

Knocking down of OXCT1-AS1 can suppress CDC25A, reduce the phosphorylation of CDK2 and induce cell cycle arrest. (A-D) Flow cytometry assays were applied to analyze the cell cycle progression of the A172 and LN229 cell lines transfected sh-OXCT1-AS1 or the vector. The cells in the different phase were assessed and showed in the bar chart. (E) The expression of cell cycle-related proteins as CDC25A, CDK2, CCNA1 and CCNE1 in OXCT1-AS1 knockdown cells. (F) Using total CDK2 as the internal controls, the expression levels of phosphorylated CDK2 were calculated. The bars represent SD (*p<0.05, **p<0.01, ***p<0.001).

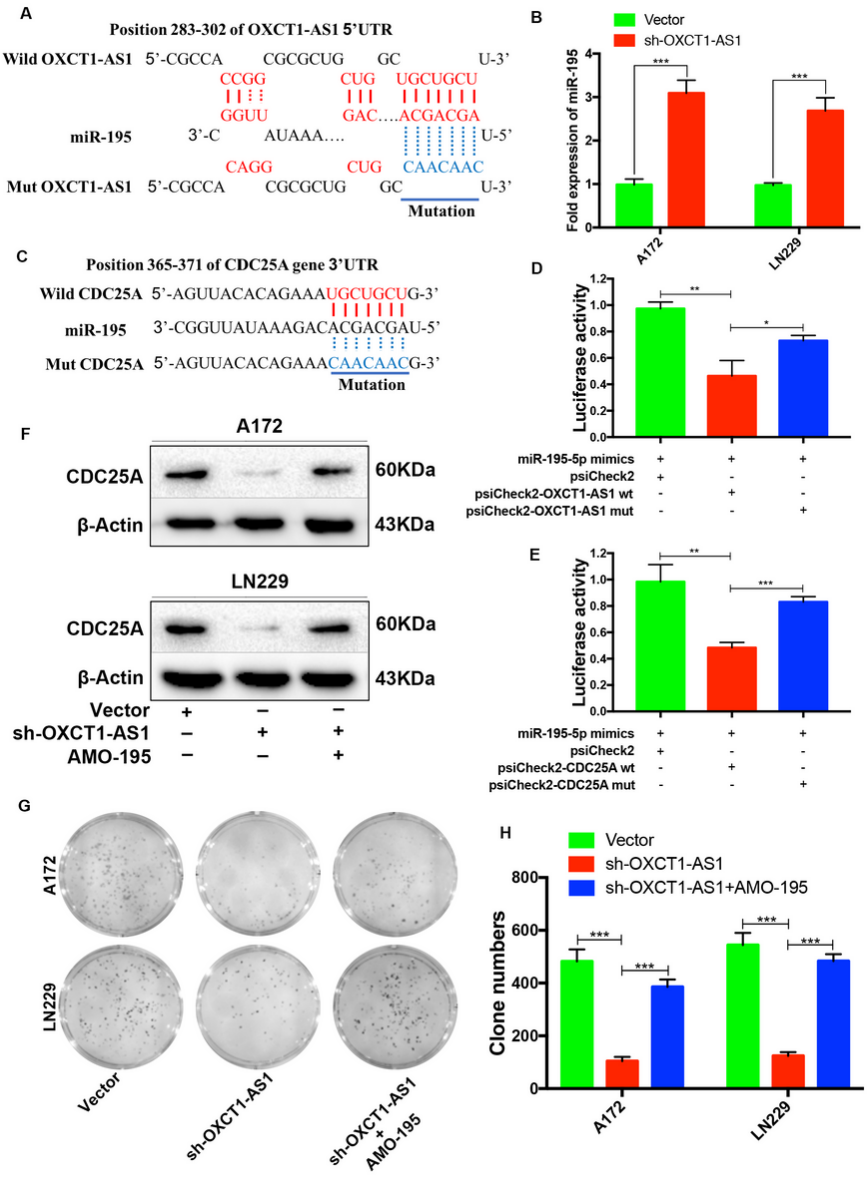

Figure 7

OXCT1-AS1 acted as a ceRNA in GBM by sponging miR-195 and releasing the downstream CDC25A. (A) The binding sequence between OXCT1-AS1 and miR-195. (B) The expression levels of miR-195 were examined by qRT-PCR assay in response to OXCT1-AS1 knockdown. (C) The binding sequence between miR-195 and CDC25A. (D) The luciferase assay was used to verify the binding between OXCT1-AS1 and miR-195. (E) The luciferase assay was used to verify the binding between miR-195 and CDC25A. (F) The western blot assay confirmed miR-195 inhibitor AMO-195 could reverse OXCT1-AS1 knockdown induced CDC25A suppression. (G, H) Colon formation assay also showed AMO-195 could partly reverse OXCT1-AS1 knockdown induced cell proliferation arrest. The bars represent SD (*p<0.05, **p<0.01, ***p<0.001).

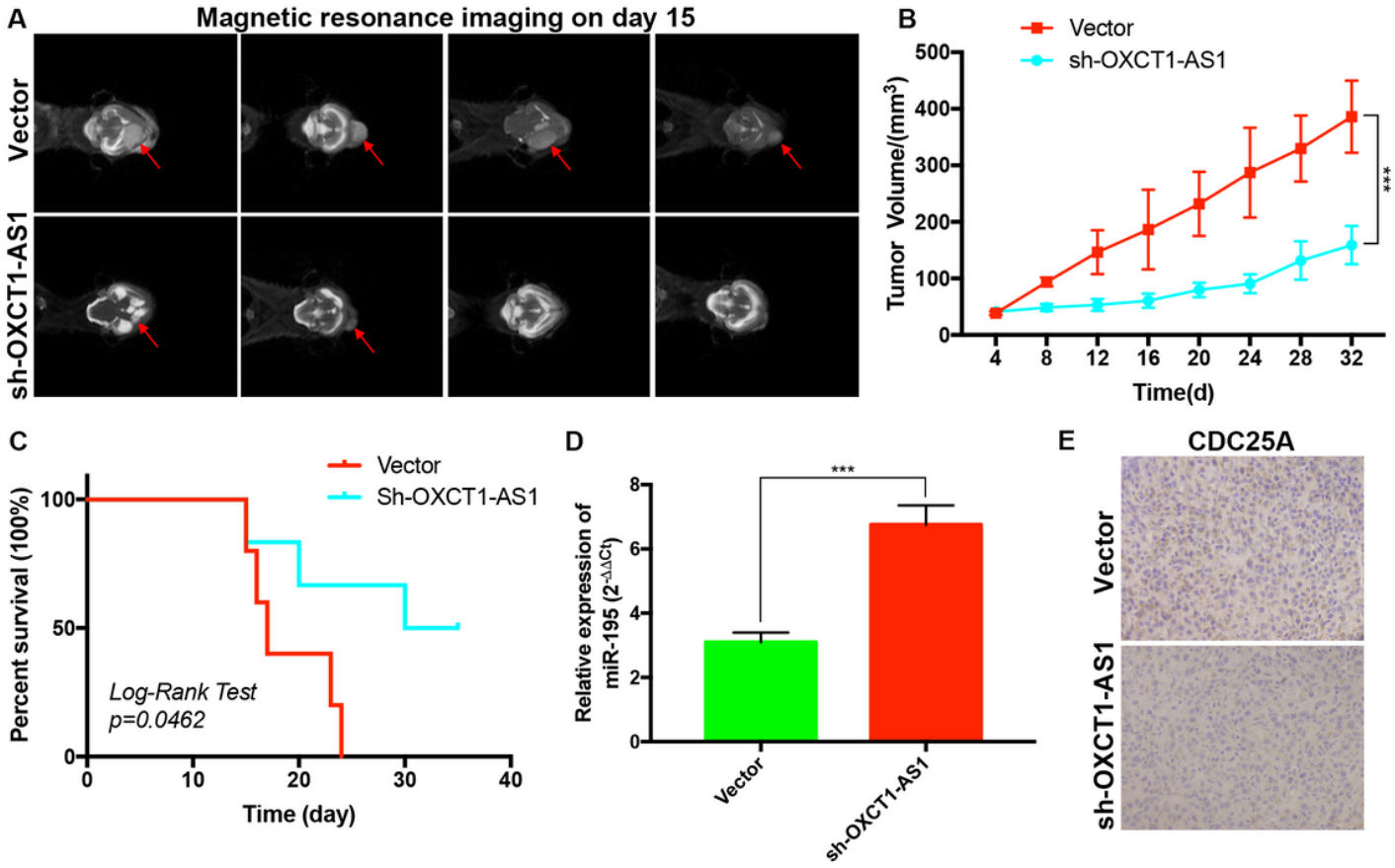

Figure 8

OXCT1-AS1 promoted the tumorigenesis of GBM cells in vivo. (A) After constructed intracranial tumors models, magnetic resonance imaging on day 15 showed the size of tumors in the sh-OXCT1-AS1 group were dramatically smaller than those in vector group. (B) Tumor volume changes were calculated every 4 days. (C) Immunohistochemistry of CDC25A in vivo. (D) The expression of miR-195 in the nude mice was detected by qRT-PCR. (E) The survival time of nude mice bearing GBM. The bars represent SD (*p<0.05, **p<0.01, ***p<0.001).

Supplementary Files

This is a list of supplementary files associated with this preprint. Click to download.

- BP.docx
- cc.docx
- mf.docx
- s1.png